ACS OMEGA

Open Access

http://pubs.acs.org/journal/acsodf

Article

Photocatalytic Hydrogen Peroxide Production from Water Using a Cyano-Covalent Organic Framework

Bernard Dawai, Ying Pan,* Patrice Kenfack Tsobnang,* Karlo Nolkemper, Ignas Kenfack Tonle, and Nieves López-Salas*

Cite This: *ACS Omega* 2026, 11, 22137−22147

Read Online

ACCESS | Metrics & More | Article Recommendations | Supporting Information

ABSTRACT: The demand for sustainable chemical production methods has led to significant advancements in photocatalysis. This study explores the photocatalytic production of hydrogen peroxide (H_2O_2) from water using a covalent organic framework (CYANO−COF) synthesized from triformylphloroglucinol (Tp) and 4,4′-diamino-[1,1′-biphenyl]-3,3′-dicarbonitrile (Bp−CN) via Schiff-base condensation. The synthesized COF material exhibited a predominantly AB stacking structure with an optimal band gap (2.22 eV) for visible-light absorption and effective charge separation. Furthermore, the photoelectrochemical characterizations revealed the photoresponsive nature of the material by creating a high charge density under illumination. Under illumination, the photocatalyst demonstrated efficient H_2O_2 generation with production rates of 550 μmolg^{-1}h^{-1} using only water and 371 μmolg^{-1}h^{-1} in the presence of ethanol. The sacrificial-agent-free system aligns with green chemistry principles, simplifying reaction conditions and reducing the environmental impact. Mechanistic studies confirmed the role of photoinduced electron−hole pairs in water oxidation and oxygen reduction. This research underscores the potential of CYANO−COF materials in sustainable H_2O_2 production using only water and sunlight thus highlighting avenues for optimizing long-term stability and efficiency.

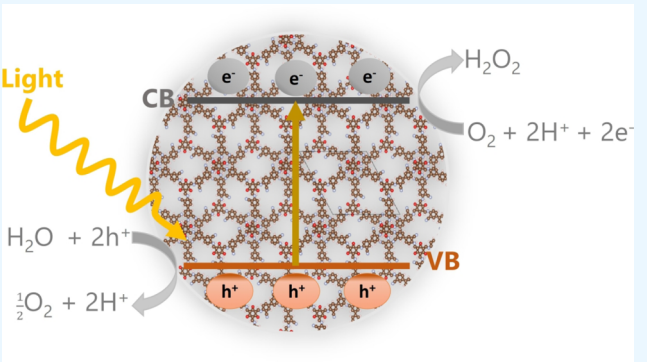

1. INTRODUCTION

The increasing demand for sustainable and environmentally friendly energy solutions has driven significant research in the field of photocatalysis.[1] Photocatalysis, which harnesses solar energy to drive chemical reactions, offers a promising avenue for producing valuable chemicals in an environmentally benign manner.[2,3] Among various photocatalytic applications, the generation of hydrogen peroxide (H_2O_2) has gained considerable attention due to its wide-ranging applications in disinfection, bleaching, and as a green oxidant in chemical synthesis.[4−6] In addition, H_2O_2 with a theoretical output power potential of 1.09 V can be used as a green fuel to generate electricity via fuel cells with zero-carbon emissions, producing oxygen and water as byproducts[7] (see Scheme 1).

Traditionally, H_2O_2 industrial production has been dominated by the anthraquinone process, a complex, multistep method involving the hydrogenation and oxidation of anthraquinone derivatives. While efficient at scale, this process is highly energy-intensive, consumes hazardous organic solvents, and generates significant chemical waste, raising serious environmental and safety concerns.[8] Moreover, the dependence on flammable gases like hydrogen and the use of pressurized reaction systems add substantial operational risks and cost to the process.[9] Many photocatalyst materials such as metal oxides, metal sulfides, graphitic carbon nitrites, and metal−organic frameworks have been used for the development of efficient, sustainable, and direct photocatalytic methods for H_2O_2 production, but their low absorption of visible light, large band gap energies, low surface area, and porosity hindered their widespread applications.[10,11] To overcome these barriers, many studies have focused on engineering the structure, band alignment, and surface chemistry of photocatalysts.[12] Many metal oxide−g−C_3N_4 heterojunctions have been developed and have efficiently produced H_2O_2 under visible light, owing to improved charge separation and extended light absorption.[13] Similarly, the introduction of single-atom metal catalysts significantly boosts H_2O_2 generation by tailoring redox reaction pathways at the atomic level.[14] Moreover, MOF-based photocatalysts had undergone modification strategies including heteroatom doping and ligand functionalization to enhance oxygen

Received: December 22, 2025
Revised: March 3, 2026
Accepted: March 5, 2026
Published: March 18, 2026

Scheme 1. Synthesis of the CYANO−COF

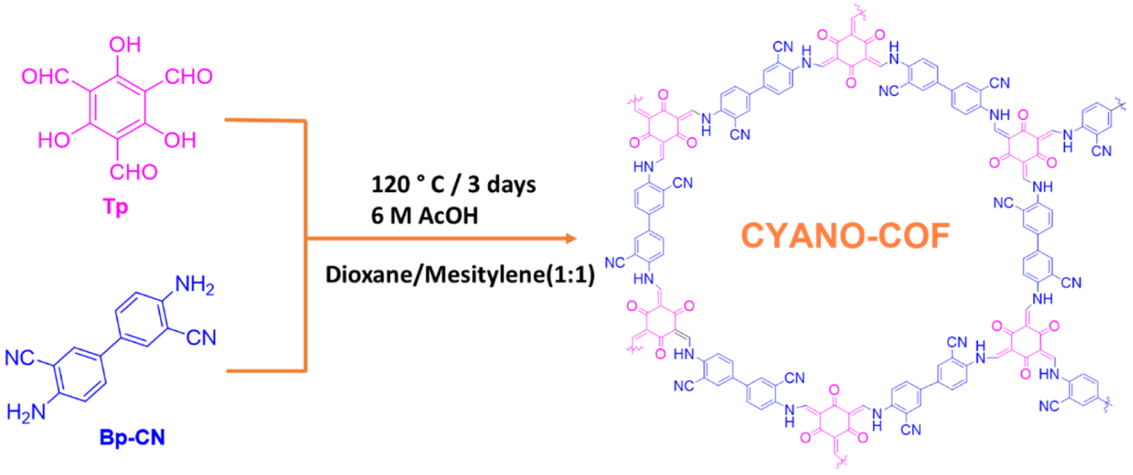

adsorption and promote selective two-electron oxygen reduction.[15]

Recent advances in photocatalytic materials have led to the exploration of covalent organic frameworks (COFs) as promising candidates for photocatalytic applications[16] due to their high surface area, tunable porosity, and structural versatility.[17] A covalent organic framework made up of electron-donor and electron-acceptor ligands showed promising properties to be used as a photocatalyst for water splitting due to their high light absorption in the visible region and low recombination of electron−hole pairs.[18−20] In addition to that, the grafting of electron-withdrawing groups, such as cyano (CN^-), fluoro (F^-), etc., greatly improved the photocatalytic properties[18] due to their ability to shift the absorption band toward the visible region and also the availability of lone pairs that increase the mobility of the photogenerated electrons within the framework of the material.

COF materials for hydrogen peroxide productions are widely used with sacrificial agents (electron donors) such as ethanol,[8,21] 2-propanol,[22] benzyl alcohol,[23,24] etc. Separating sacrificial agents from the mixtures becomes very difficult since hydrogen peroxide decomposes at low boiling temperatures.[25,26] The production rate of hydrogen peroxide from pure water was low.[27,28] In this view, developing photocatalyst materials for hydrogen peroxide production from water and exhibiting a higher production rate is an endeavor.

Triformylphloroglucinol (Tp) is a commonly used building block in COF synthesis due to its propensity to form β-ketoenamine linkages through Schiff-base condensation under solvothermal conditions.[18] Tp's aromatic backbone promotes π-conjugation, facilitating light absorption and charge transfer, which is essential for photocatalysis. When combined with 4,4′-diamino-[1,1′-biphenyl]-3,3′-dicarbonitrile (Bp−CN), a nitrogen-rich aromatic amine with strong electron-donating characteristics, the resultant COF has an expanded π-system, improved light harvesting, and increased electron mobility.[19] Tp introduces electron-withdrawing centers via its carbonyl groups, whereas Bp-CN adds electron-rich nitrile groups. The electron donor−acceptor (D−A) architecture facilitates photoinduced electron transfer, a process essential for efficient H_2O_2 synthesis during water splitting.[29] The nitrile groups of Bp−CN also contribute to the hydrophilicity of the COF, which allows for improved contact with the water molecules required for photocatalytic activity. Furthermore, the CYANO−COF has inherent catalytic benefits for H_2O_2 production. First, its highly ordered and crystalline structure allows for effective separation and migration of photogenerated charge carriers, reducing recombination losses. Second, its visible-light activity and appropriate band gap (between 2 and 3 eV) are consistent with the solar spectrum, maximizing photon use.[30]

This research explores the use of a CYANO−COF for the photocatalytic production of hydrogen peroxide through water splitting without the need for sacrificial electron donors. This approach simplifies the reaction system and aligns with the principles of green chemistry by using only water and sunlight. The objectives of this study are to synthesize and characterize the COF material based on triformylphloroglucinol (Tp) and 4,4′-diamino-[1,1′-biphenyl]- 3,3′-dicarbonitrile (Bp−CN), determine its stacking model via simulation methods, study its photoelectrochemical properties, evaluate its photocatalytic performance for H_2O_2 production, elucidate the mechanism governing the process for producing hydrogen peroxide, and study the effect of different scavengers on the production rate of H_2O_2. The synthesized CYANO−COF material shows a suitable band gap energy for photocatalytic activities and exhibits charge separation on its surface under illumination. The study of the mechanism reveals that the H_2O_2 generation is done via two methods: the water oxidation reaction (WOR) and the oxygen reduction reaction (ORR).

2. MATERIALS AND METHODS

2.1. Reagents and Solvents

All the chemicals were of analytical grades, purchased from commercial sources, and were used without further purification. Triformylphloroglucinol (Tp, 98%, TCI), 4,4′-diamino-[1,1′-biphenyl]- 3,3′-dicarbonitrile (Bp−CN, 97%, Sigma-Aldrich), dioxane (99%, Sigma-Aldrich), mesitylene (98%, Sigma-Aldrich), acetic acid (100%), acetone (100%), tetrahydrofuran (THF, 99.9%, Sigma-Aldrich), dimethylformamide (DMF, 99.8%, Sigma-Aldrich), potassium iodide (99.5%, Merck), ammonium heptamolybdate tetrahydrate (AHMTH, 99%, Sigma-Aldrich), ethanol (100%), pure hydrogen peroxide (35%), sodium sulfate anhydrous (99%, Molychem), potassium chloride (99%, Sigma-Aldrich), *p*-benzoquinone (pBQ, 98%, Thermo scientific), ethylenediamine tetraacetic acid disodium salt dehydrate (EDTA-2Na, Supelco), and Isopropyl alcohol (IPA, 100%) were used.

2.2. Synthesis of CYANO−COF

The synthesis procedure is inspired by the work done by Li et al.[30] In brief, 84 mg (0.4 mmol) of Tp and 141 mg (0.6 mmol) of Bp−CN were loaded into a 25 mL Teflon reactor, and 6 mL (1:1 wt %) of

https://doi.org/10.1021/acsomega.5c13395
ACS Omega 2026, 11, 22137−22147

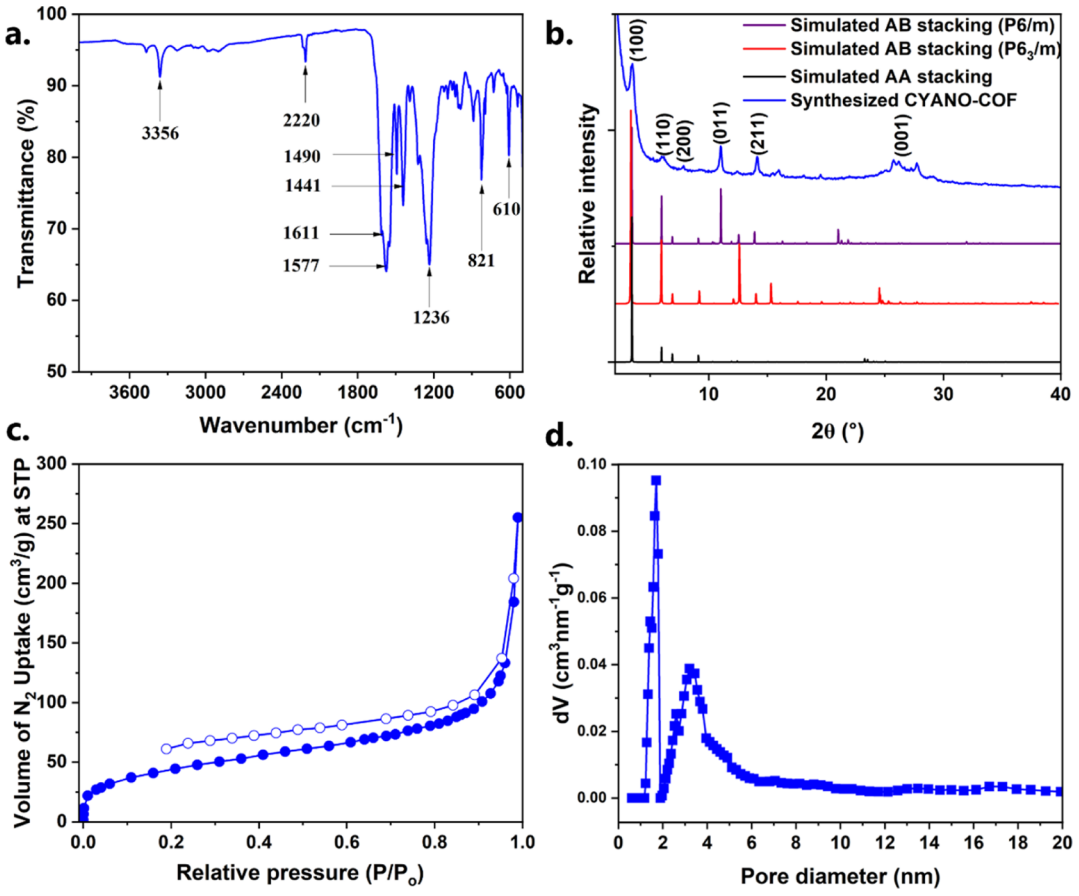

Figure 1. a) FTIR, (b) powder XRD patterns of simulated AB stacking compared to the synthesized CYANO−COF, (c) nitrogen sorption isotherm, and (d) pore size distribution curve of synthesized CYANO−COF.

mesitylene and dioxane mixture was added. The solution was sonicated for 10 min. Two mL of 6 M acetic acid was added, and the mixture was further sonicated for 10 min. Nitrogen was purged into the suspension for 5 min. The Teflon reactor was put into an autoclave and then placed into a 120 °C preheated oven for 3 days. The solid obtained was filtered and washed with DMF, acetone, and THF. After that, the solid was soaked in acetone for 5 days and then dried in a vacuum oven at 120 °C for 12 h. An orange crystalline powder of mass 192 mg was collected given a percentage yield of 85%. The scheme below shows the equation of the reaction.

2.3. Physicochemical Characterization

A Bruker D8 Advance diffractometer equipped with a Cu K_α X-ray source measuring 2θ from 0.55° to 80° was used to obtain the powder diffraction patterns. The ATR-FTIR measurements were performed at room temperature on FTIR Spectrometer Spectrum Two from PerkinElmer GmbH using the PerkinElmer Spectrum IR Program in which the spectrum was recorded in transmission mode in the range 400−4000 cm^{-1}. The morphologies of the samples were characterized by Scanning Electron Microscopy (SEM, Zeiss Neon 40). The nitrogen sorption measurement was carried out with an Autosorb 6 from Quantachrome at −196 °C. For the pretreatment of the sample for the sorption measurement, 0.021 g of the CYANO−COF was used and the degas was done at a temperature of 100 °C for a duration of 6 h. The specific surface areas were calculated by using the Brunauer−Emmett−Teller (BET) method applied to nitrogen adsorption data (p/p_0) with the Rouquerol criteria. The pore size distribution of the material was obtained by applying the Non-Localized Density Functional Theory (NLDFT) method with slit/cylindrical/sphere pore shape to the adsorption branch of nitrogen isotherms. The two-beam spectrometer (Lambda 650) from PerkinElmer was used to measure the optical property of the material by recording the absorbance in the range of 200−800 nm, and a liquid UV−visible spectrophotometer (PerkinElmer, Lambda 19) was used for the quantification of hydrogen peroxide by recording the absorbance of the solution contained in a 1 cm width quartz cuvette within a wavelength range of 250 to 600 nm. A white light lamp of power 50 W was used as a light source for photocatalysis.

2.4. Photoelectrochemical Characterization

2.4.1. Electrode Preparation. Two mg portion of CYANO−COF was dispersed into a mixture of ethanol (0.5 mL) and Nafion (10 μL). The suspension obtained was then deposited onto the surface of an ITO glass (0.8 × 1 cm), which was used as the working electron for the different measurements. The electrolyte solution used was 0.25 M Na_2SO_4, the reference and counter electrodes being Ag/AgCl and Pt, respectively.

2.4.2. Measurements. The measurements were taken using a PalmSens3 potentiostat and PStrace4 software. Cyclic voltammetry (CV) was performed at a scan rate of 50 mV/s in the potential range of −0.2 and 0.6 V. The electrochemical impedance spectroscopy (EIS) was measured at a fixed potential of 0.6 V using a scan frequency of 0.1 to 1000 Hz with an equilibrium time of 240 s. Linear sweep voltammetry (LSV) was performed at a potential range of 0 to 0.6 V with a scan rate of 50 mV/s. The chronoamperometry (CA) and Mott Schottky (MS) measurements were run using a Gamry potentiostat. The CA measurements were performed using an applied potential of 0.6 V for a period of 240 s with an off and on light interval of 20 s. For the MS, the prepared ink was deposited on the glassy carbon, and different frequencies (0.5 1, 1.5, and 2 kHz) were used to perform the measurements.

2.5. Photocatalytic Hydrogen Peroxide Production and Analysis

2.5.1. Experiment. In a typical photocatalytic experiment, 10 mg of the photocatalyst was dispersed in 20 mL of deionized water (with

https://doi.org/10.1021/acsomega.5c13395
ACS Omega 2026, 11, 22137−22147

an additional 2 mL of sacrificial agent or scavenger when applicable) in a 50 mL vial. The vial was covered with parafilm paper, and air was purged for 5 min. The solution obtained was transferred into a photoreactor vessel connected to a cooling system. 1.5 mL of the liquid is removed and centrifuged every hour. The H_2O_2 test trips were dipped into the reaction solution to roughly check the production rate of H_2O_2. The blue coloration of different intensities corresponding to the amount of H_2O_2 produced was observed after an increasing time of illumination (Figure S1).

For the quantitative analysis of the H_2O_2 produced, 1 mL of the centrifuged suspension is mixed with 2 mL of 0.1 M aqueous solution of potassium iodide (KI) and 50 μL of 0.01 M aqueous solution of ammonium heptamolybdate tetrahydrate (AHMTH). The obtained solution was diluted 6 times by mixing 0.5 mL of the above mixture with 2.5 mL of distilled water. The diluted solution was then analyzed using UV−visible spectroscopy and the concentration of the H_2O_2 was determined from the calibration curve (Figure S2a) obtained from the analysis of pure hydrogen peroxide at the wavelength of 352 nm (Figure S2b).[31] The experimental setup is given in Scheme S1.

2.5.2. Hydrogen Peroxide Quantification Method. The equations below show the different chemical reactions involved in determining the amount of hydrogen peroxide produced.[32]

$$2H_2O + \frac{1}{2}O_2 \rightarrow H_2O_2 \quad (1)$$

$$H_2O_2 + 2I^- + 2H^+ \rightarrow I_2 + 2H_2O \quad (2)$$

$$I_2 + I^- \rightarrow I_3^- \quad (3)$$

The mixing of 1 mL of the centrifuged suspension with 2 mL of 0.1 M KI and 50 μL of 0.01 M AHMTH gave a yellow solution which is the characteristic color of triiodide (I_3^-) and this species has two characteristics absorption wavelengths at 288 and 352 nm.[32] From eqs 1, 2, and 3, the amount of I_3^- formed is directly related to the amount of H_2O_2 produced. The concentration of hydrogen peroxide in millimolar per gram catalyst ($mmolg_{cat}^{-1}$) and the rate of hydrogen peroxide production in micromole per gram catalyst per hour $\mu molg_{cat}^{-1}h^{-1}$ are gotten from the expressions (eq 4 and eq 5):

$$\frac{[H_2O_2]}{\text{mass of catalyst}} = \frac{6000C}{m} \quad (4)$$

$$\text{Initial rate} = \frac{V \times [H_2O_2]}{h} \quad (5)$$

where V is the volume of solution (water only or the mixture of water and ethanol) in mL, h the hour of illumination, m the mass of the photocatalyst used in mg, C is the concentration(μM) of triiodide derived from eq 6 of the line of the calibration curve.

The equation is

$$C = \frac{A - b}{a} \quad (6)$$

where A is the absorbance intensity, b is the y-intercept, and a is the slope of the curve.

3. RESULTS AND DISCUSSION

3.1. Physicochemical Properties

The physicochemical properties of the synthesized material were determined using the techniques FT-IR, PXRD, nitrogen isotherms, SEM, and solid UV visible analysis. Figure 1a shows the FTIR spectrum of the synthesized CYANO−COF revealing the different functional groups expected in the material. The vibration peaks at 3356, 1611, 1577, and 1236 cm^{-1} are, respectively, assigned to the N−H, C═O, C═C, and C−N stretching vibrations. These peaks, together with aromatic ring skeleton vibrations observed at 1490 and 1441 cm^{-1}, show the formation of β-ketoenamine linkage.[30] The C≡N stretching vibration appears at 2220 cm^{-1}, indicating that cyano groups can endure the synthesis conditions without decomposition. The absorption bands at 610 and 821 associated with the out of plane C−H bend of a benzene 1,2,4-trisubstituted further confirm the presence of the Bp−CN moiety. The crystalline structure of the synthesized material was investigated by using powder X-ray diffraction (PXRD), as shown in Figure S3a. A prominent diffraction peak appears at 2θ = 3.51°, corresponding to the (100) reflection plane, while additional peaks of lower intensity are observed at 6.08° and 7.81°, which can be assigned to the (110) and (200) planes, respectively. These reflections are consistent with values reported in the literature.[30] A broad peak between 25° and 30°, similarly reported in earlier studies,[30] is attributed to the (001) reflection and indicates the stacking of 2D layers in the COF.

To investigate the stacking arrangement, PXRD patterns were simulated for both eclipsed AA and staggered AB stacking models using a hexagonal lattice with space group $P6/m$ and unit cell lattice parameters $a = b = 29.6547$ Å, $c = 8.44471$ Å, $\alpha = \beta = 90$, and $\gamma = 120$ with an average interlayer space of 3.97 Å for AB and 3.82 Å for AA stacking models (the VESTA simulated view is given in Figure S4). The experimental PXRD pattern of the synthesized material aligns more closely with the staggered AB stacking model as the major peaks are well matched and can be clearly identified (Figure 1b). Notably, reflections at 11.04° and 14.18°, corresponding to the (011) and (211) planes, respectively, are present in the synthesized sample but absent in the reported CYANO−COF with an eclipsed AA stacking configuration. In contrast, the comparison with the simulated AA stacking model reveals a poor correlation. This result suggests that the synthesized CYANO−COF may consist of a mixture of stacking phases, with a predominant tendency toward a staggered AB stacking mode. This configuration differs from previously reported AA-stacked structures and the idealized AB stacking model (space group $P6_3/m$) described in earlier studies.[30]

The nitrogen sorption isotherm measured at 77 K (Figure 1c) exhibits a combination of type I and type II characteristics according to the IUPAC classification, indicating the coexistence of micro- and mesopores in the synthesized material. The corresponding pore size distribution curve (Figure 1d), calculated using the nonlocalized density functional theory (NLDFT) model, reveals that the material is predominantly microporous, with a pore width centered between 1 and 2 nm, consistent with the simulated pore width (Figure S5). A smaller fraction of mesoporous-like pores in the range of 2 to 6 nm is also observed. The average pore width is calculated to be 1.696 nm, with a pore volume of 0.227 cm^3g^{-1}, based on the NLDFT model. These features suggest that the material preferentially adopts an AB stacking mode, which is in good agreement with both the simulated and the experimental PXRD patterns. The Brunauer−Emmett−Teller (BET) surface area of the synthesized CYANO−COF is determined to be 202 m^2g^{-1}. This value, lower than the one reported in the literature[30] (559 m^2g^{-1}), can be due to the phase mixture and predominantly staggered AB stacking model as observed with powder XRD patterns, which reduces surface accessibility due to the offset arrangement of the layers.[33] The morphology of the material was observed by using SEM (Figure S6). This material exhibited a needle-like morphology similar to the one reported in the literature.[30]

https://doi.org/10.1021/acsomega.5c13395
ACS Omega 2026, 11, 22137−22147

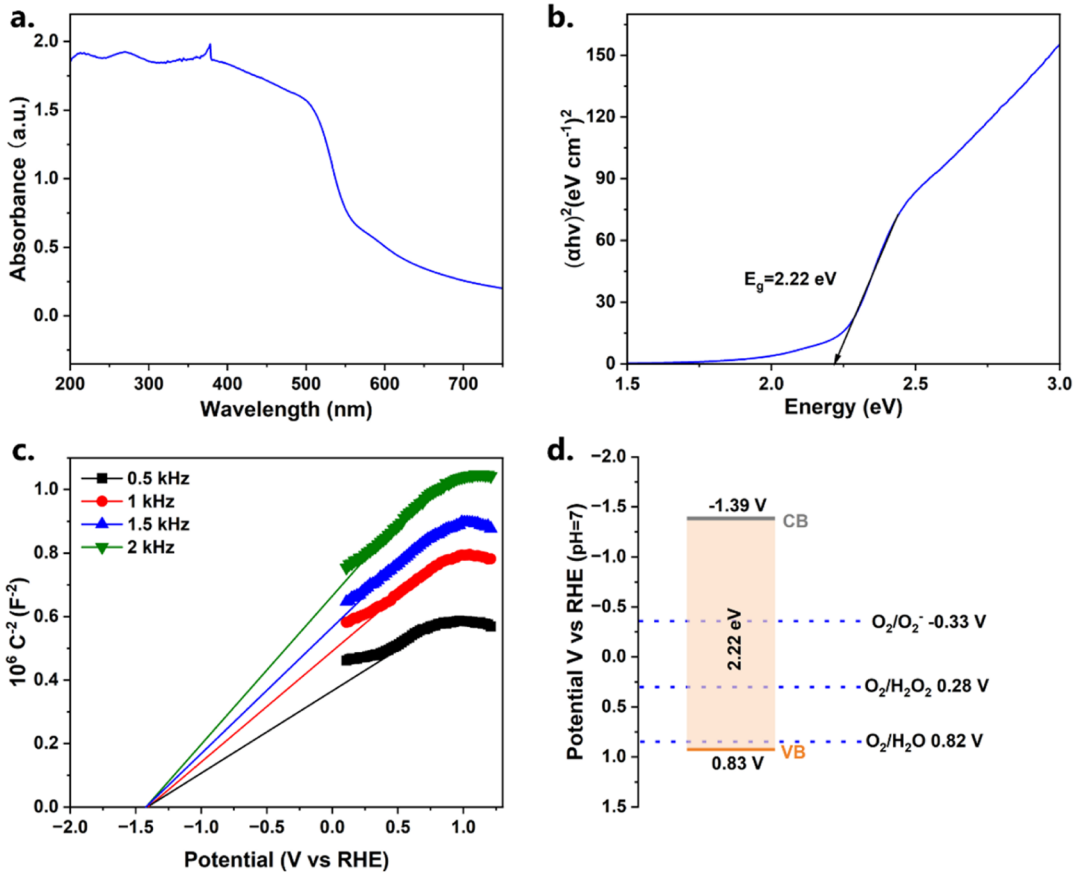

Figure 2. a) Solid UV−visible spectrum of the synthesized CYANO−COF, (b) Tauc plot for optical band gap estimation, (c) Mott−Schottky plots, and (d) approximated conduction and valence band positions of the synthesized CYANO−COF.

Figure 2a shows the UV−visible diffuse reflectance spectrum of the synthesized CYANO−COF, which exhibits strong absorption in the UV and visible region up to 600 nm. The optical band gap energy of this material was calculated to be 2.22 eV using the Tauc plot (Figure 2b), a value slightly higher than the one reported (2.17 eV).[30] A similar observation was made by Li and Co., in which they synthesized an imine-based COF with AA and AB stacking models, with the AB stacking model having a wider optical band gap (2.19 eV) energy than the AA model (2.15 eV), and this was associated with the reduction in $\pi-\pi$ orbital overlap in the AB mode.[34] Figure 2c presents the Mott−Schottky measurements recorded at frequencies of 0.5, 1.0, 1.5, and 2.0 kHz, which were used to determine the flat band potential of the CYANO−COF. For this n-type semiconductor, the flat band potential was employed as an approximation of the conduction band minimum.[30,35] Accordingly, the conduction and valence band positions of the synthesized CYANO−COF were estimated to be −1.39 and +0.83 V vs RHE at pH = 7, respectively, as shown in Figure 2d, which are markedly shifted compared with the reported AA-stacked CYANO−COF (−0.89 and +1.28 V). While both materials possess comparable optical band gaps (∼2.2 eV), the synthesized CYANO−COF exhibits a significantly more negative conduction band and a less positive valence band. This indicates that electrons in material possess stronger reducing power, favoring the two-electron reduction of O_2 to H_2O_2 (E° = +0.28 V vs RHE), whereas the oxidative ability of photogenerated holes is correspondingly diminished, rendering water oxidation thermodynamically less favorable. The observed shift can be attributed to the electronic influence of AB stacking, where the staggered arrangement of adjacent layers enhances $\pi-\pi$ delocalization of LUMO states and stabilizes conduction-band electrons while slightly destabilizing the HOMO.

3.2. Photoelectrochemical Properties

The photogenerated charge separation and recombination behavior were explored by testing the photocurrent response of the synthesized material under illumination and in the dark. The CV spectra (see Figure 3a) show that the material exhibits reversible photocurrent responses under light and in the dark, with the photocurrent density greater when illuminated than in the dark. Light significantly promotes the transfer and generation of photogenerated electron−hole pairs. The electrochemical impedance spectroscopy illustrates that the material under illumination appears as the smaller arc in the Nyquist plot (see Figure 3b), manifesting lower charge resistance in the material contributing to the rapid transport and separation of photoproduced charges.[36] However, in the absence of light, the material exhibited a larger arc under the same conditions, indicating that the lack of light inhibits the transfer of photocarriers due to the interface resistance. Also, it can be observed from the LSV curves (see Figure 3c) that the illumination can significantly increase the cathodic current density compared to the dark, demonstrating that the CYANO−COF material can achieve faster surface kinetic reactions and effective photogenerated charge separation when illuminated. To further confirm the efficient charge separation behavior of the material, photocurrent response measurements

https://doi.org/10.1021/acsomega.5c13395
ACS Omega 2026, 11, 22137−22147

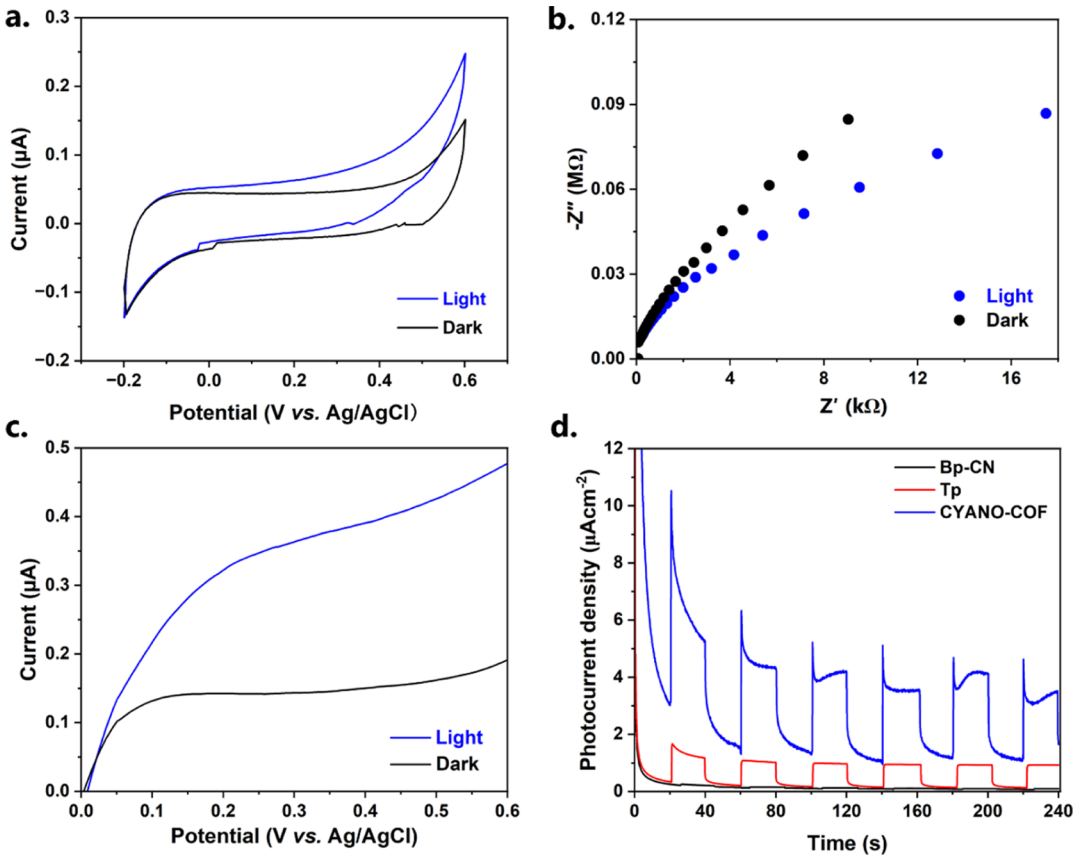

Figure 3. Photoelectrochemical properties of CYANO−COF in 0.25 M Na_2SO_4 electrolyte solution under illumination and without illumination using Ag/AgCl. (a) Cyclic voltammograms, (b) electrochemical impedance spectroscopy plots, (c) linear sweep voltammograms, and (d) transient photocurrent decay of Tp, Bp-CN, and CYANO−COF.

were conducted for the synthesized CYANO−COF and the precursor ligands. The transient photocurrent response curves (Figure 3d) clearly demonstrate enhancement in photocurrent for CYANO−COF indicating more efficient photoinduced charge separation and transport, which can be attributed to the extended π-conjugation, improved crystallinity, and the presence of electron-withdrawing cyano groups within the framework. The fast rise and decay of the photocurrent under light on/off switching also suggest good photostability and reversibility of the CYANO−COF system. In contrast, the ligand precursors show weaker and slower photocurrent responses, underlining their limited capability for efficient charge carrier dynamics when used alone. Furthermore, to support this, CV and EIS (see Figure S7a,b) of the precursors were conducted, and they showed lower current density and larger arcs, respectively, than the CYANO−COF. These results indicate that illumination can accelerate the generation, separation, and migration of photogenerated charges, thereby allowing high photocatalytic water splitting for hydrogen peroxide production.

4. PHOTOCATALYTIC HYDROGEN PEROXIDE PRODUCTION

4.1. Production Rates of H_2O_2 with Water and Water/Ethanol Mixture (10/1) by the CYANO−COF

Figure 4a shows the photocatalytic hydrogen peroxide production test using water and ethanol (black curve), the CYANO−COF mixed with water and ethanol (red curve), and the CYANO−COF mixed with water only (blue curve). The illumination of the mixture of water and ethanol shows no characteristic absorption band of triiodide at 352 nm. Meanwhile, the mixtures involving the CYANO−COF material show the absorption bands attributed to the triiodide ions, thus confirming the generation of the hydrogen peroxide. These results show that the CYANO−COF-photocatalyzed water-splitting reaction leads to the formation of hydrogen peroxide. It is also noted that the absorbance of the triiodide ions is higher for the mixture of CYANO−COF with water than that of the mixture of ethanol, water, and the material. The lower amount of the H_2O_2 produced using ethanol can be ascribed to the strong surface adsorption of ethanol on the material through hydrogen bonding or coordination with the framework's functional sites (imine-, hydroxyl-, or oxygen-containing moieties). Therefore, ethanol molecules can be adsorbed and partially cover the active sites of the COF, leading to surface passivation that restricts the interaction between water molecules and the photoactive centers. This competitive adsorption between water and ethanol limits water oxidation and, thereby, suppresses H_2O_2 formation. Similar behavior has been reported in photocatalytic systems where ethanol adsorption hinders charge transfer and active-site accessibility.[37−40]

The photocatalytic hydrogen peroxide generation was evaluated for a longer period of up to 5h as given in Figure 4b (with the UV visible analysis given in Supporting Information Figure S8), and it revealed that the amount of hydrogen peroxide produced is directly proportional to the illumination time. This direct relationship can be associated

https://doi.org/10.1021/acsomega.5c13395
ACS Omega 2026, 11, 22137−22147

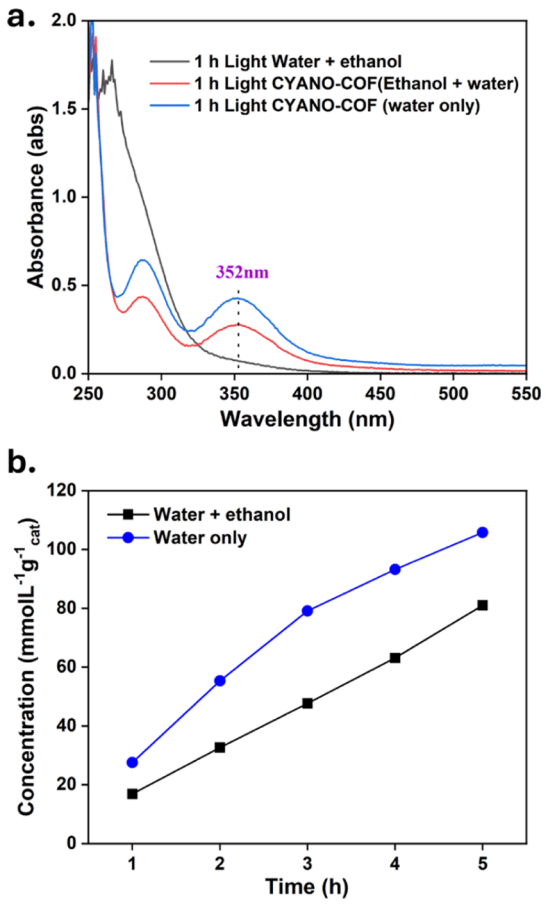

Figure 4. Hydrogen peroxide production of (a) 1 h illumination of water + ethanol, CYANO−COF (water + ethanol), and CYANO−COF (water only). (b) Concentration of hydrogen peroxide per gram catalyst at a given time interval.

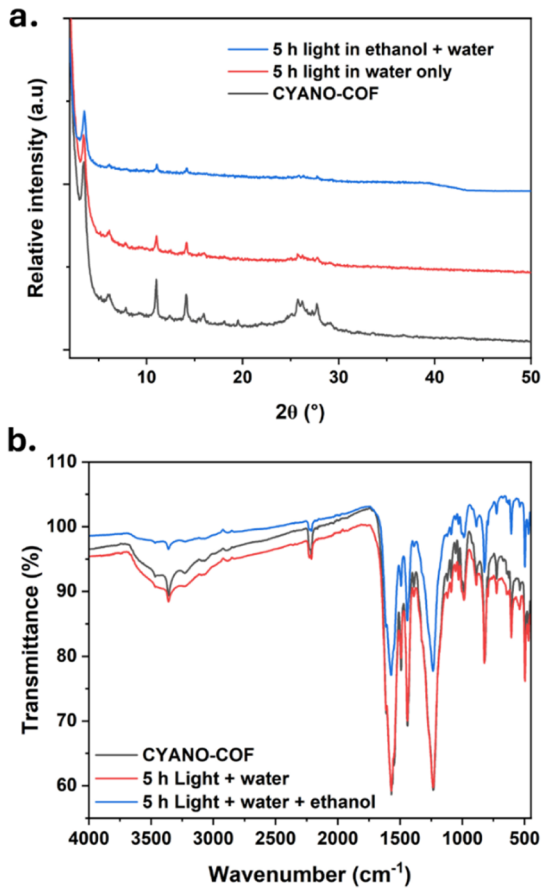

Figure 5. a) Powder XRD patterns and (b) FT-IR spectra of CYANO−COF before and after production of H_2O_2 from ethanol/water (1/10) and in water only for 5 h illumination.

with the structural stability of the material, as observed by the retention of the predominant peaks on the PXRD patterns after the photocatalytic processes (Figure 5a). The hydrogen peroxide production rates are calculated to be 550 μmolg^{-1}h^{-1} and 371 μmolg^{-1}h^{-1} when only water and water with ethanol were used as precursors, respectively. Two more photocatalytic cycle experiments were performed using only water, and the production rate at each interval time is similar (Figure S9). The production rates exceed some of those reported for certain COF-based photocatalysts and other classes of photocatalysts such as graphitic carbon nitrides and oxide materials (Tables 1 and 2). The solar-to-chemical conversion (SCC) and the apparent quantum efficiency (AQE) are calculated to be 0.13% and 0.65%, respectively. These values are comparable to a reported imine TZ-COF material with SCC and AQE of 0.036% and 0.6%, respectively.[41] These findings suggest that the synthesized material holds the potential for use in photocatalytic hydrogen peroxide production from water under visible-light irradiation. While the overall activity remains modest compared to the most advanced COF-based systems, the process benefits from its environmental friendliness and the use of only water and visible light. To further confirm that the synthesized material is responsible for the photocatalytic process, hydrogen peroxide production experiment was tested with the ligands and the UV−visible spectra given in Figure S10 of the Supporting Information. No absorbance band was observed with the ligand Bp−CN meant, while with the ligand Tp, we observed one band at around 352 nm. The test trip was performed and a yellow coloration (different from blue which is confirmation test) was obtained; this suggest that no H_2O_2 was produced and that different product was formed. This result shows that the hybrid formed by combining a donor and an acceptor molecule promotes photoinduced charges responsible for H_2O_2 production which is in accordance with the inherent photoelectrochemical properties of the ligands which shows lower photocurrent density and larger arc circles in EIS compared to the material formed (Figure S7).

To confirm the role of light in this process, the material and water mixture was stirred for one hour and the solution was analyzed using liquid UV−visible (Figure S11). The spectrum shows an absence of the 352 nm band associated with the triiodide ion, thus indicating that stirring did not contribute to the process and only light induced the reaction for hydrogen peroxide production. In addition to this, dark control experiments were conducted to evaluate the contributions of the scavenger (Figure S12); from this, no peak was observed at 352 nm, thus confirming that only the material in the presence of light is responsible for the H_2O_2 production.

Photocatalytic hydrogen peroxide production using direct sunlight was carried out for 1 h illumination and tested using the test trip (Figure S13). The test strip showed the blue characteristic color of the H_2O_2; this shows that sunlight can generate H_2O_2 from water when using the material. The enhanced charge separation leading to H_2O_2 production can be

https://doi.org/10.1021/acsomega.5c13395
ACS Omega 2026, 11, 22137−22147

Table 1. Comparison of the Production Rate with Existing COF Materials

photocatalyst	surface area (m^2/g)	irradiation condition	sacrificial agent	H_2O_2 generation rate ($\mu molg^{-1}h^{-1}$)	AQE %	ref
CYANO−COF	202	white light	H_2O	550	0.65	this work
			H_2O/EtOH (10:1)	371		
TAPD-$(Me)_2$	1083	400−700	H_2O/EtOH (9:1)	234	N/A	8
CTF-BDDBN	34.1	>420	H_2O	70	N/A	19
TiCOF-spn	621.38	>420	H_2O/EtOH (9:1)	489	N/A	51
SonoCOF-F2	1425	>420	H_2O	197	4.8	52
TZ-COF			H_2O/MeOH (1:1)	268	0.6	41

AQE: Apparent Quantum Efficiency, N/A: Not Acquired.

Table 2. Comparison of Production Yield with Other Reported Materials

material	sacrificial agent	concentration of catalyst	irradiation condition	H_2O_2 yield	ref
CYANO−COF	H_2O	0.5 mg/mL	white light	1.1 mmol (2 h)	this work
	H_2O/EtOH (10:1)			652.9 μmol (2 h)	
Au/g-C_3N_4	2-propanol	1 mg/mL	UV/vis	747 μmol (2 h)	53
TiO_2	2-propanol	1 mg/mL	>365	423.2 μM (2 h)	54
resins	water	50 mg/30 mL	>420	99 μmol (24 h)	55
graphene oxide	water	0.32 mg/20 mL	>420	200 μM (1 h)	56

attributed to the AB stacking mode which introduces an interlayer offset that spatially separates the π-electron systems of adjacent layers and thus reduces charge recombination probability. Previous DFT studies have shown that AB stacking lowers the total energy and promotes anisotropic charge transport.[42]

4.2. Reusability of CYANO−COF for H_2O_2 Production

The reusability of the photocatalyst was studied by performing a second round of five hour illumination. Figure S14 shows hydrogen peroxide concentrations before and after the first photocatalytic activity with only water. From the figure, the production rate after the first round of photocatalysis is higher than the second round; this shows that the material can be reused to a certain extent. This observation may be associated with structural changes induced by prolonged light irradiation. PXRD analysis after photocatalysis (Figure 5a) shows that the diffraction peaks corresponding to the COF are largely preserved, confirming that the overall layered structure remains intact. However, the broad diffraction feature in the 25°−30° range, assigned to the (001) reflection, becomes noticeably weakened and broadened after irradiation, suggesting a partial loss of long-range interlayer ordering or reduced stacking coherence rather than a change in stacking mode. Such changes in stacking-related reflections are commonly associated with increased stacking disorder and have been reported for layered COFs subjected to external stimuli.[43,44] Figure 5a shows the FTIR spectra of the material after photocatalysis under different conditions. From this, we observe no change in the positions of the absorption bands, suggesting that the chemical composition was not affected during the catalytic process.

5. PROPOSED MECHANISM FOR HYDROGEN PEROXIDE GENERATION

The photocatalytic hydrogen peroxide production mechanism over the surface of the CYANO−COF was studied by carrying out the production process in nitrogen (N_2) gas, air (open system), and a closed system (sealed system). Figure 6a shows the concentration of hydrogen peroxide produced under the different conditions. In N_2, the concentration of the H_2O_2 is 16.0 $\mu molL^{-1}$ lower than that in air (255 $\mu molL^{-1}$ and 312 $\mu molL^{-1}$ for sealed and open systems) (see Figure S15); this could indicate that water oxidation reaction might occur on the positive hole sites created after illumination and which via two electron reduction process the oxygen produced is reduced to H_2O_2. The low concentration can be associated with the band structure of the material, in which the valence band potential is slightly lower than the water oxidation reaction potential (Figure 2b). The concentration of hydrogen peroxide

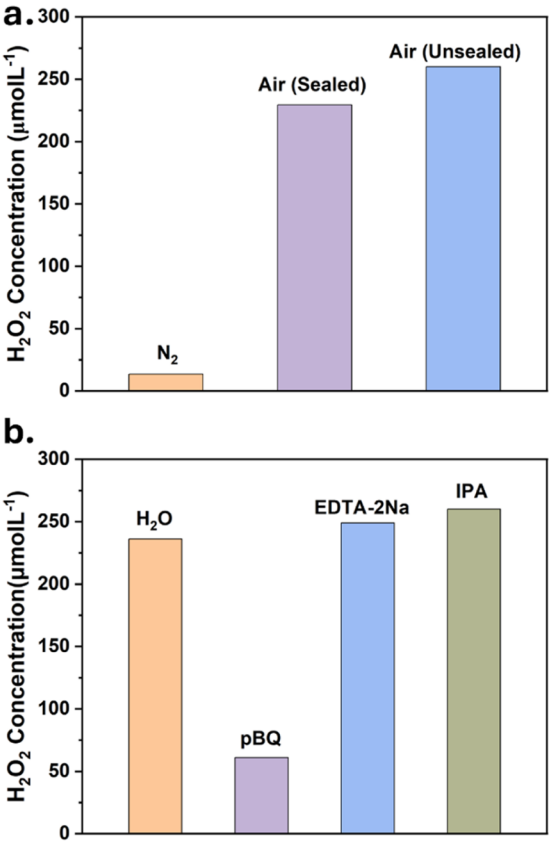

Figure 6. a) Photocatalytic hydrogen peroxide production in different conditions. (b) Comparison of hydrogen peroxide concentrations using different scavengers after 1 h illumination.

https://doi.org/10.1021/acsomega.5c13395
ACS Omega 2026, 11, 22137−22147

produced in an open and sealed system was evaluated, with the concentration higher in an open system; this can result from a continuous supply of oxygen gas in the open system. The mechanism can be ascribed to two routes; first, photocatalytic water oxidation reaction, in which photogenerated holes oxidize water to oxygen (eq 7), and second, oxygen reduction reaction in which the photogenerated electrons reduce oxygen to hydrogen peroxide (eq 8). This proposed mechanism was also reported in the literature.[28,45]

$$H_2O + 2h^+ \rightarrow \frac{1}{2}O_2 + 2H^+ \quad (7)$$

$$O_2 + 2H^+ + 2e^- \rightarrow H_2O_2 \quad (8)$$

Furthermore, the effect of different scavengers on the photocatalytic process was investigated, and Figure 6b shows the concentration of the peroxide produced (the UV−visible spectra in different scavengers are given in Figure S16). The amount of the hydrogen peroxide produced using EDTA-2Na is higher than that of water only. EDTA-2Na is reported to act as a hole scavenger and therefore this observation can be attributed to the reduction of the recombination sites, causing more electrons to be available and thus increasing the photoactivity.[46] Also, IPA, known as a hydroxyl radical (·OH)-trapping agent,[45,47] was used and had the highest production performance. This indicates that the ·OH radicals did not participate in the photocatalytic reaction. The pBQ is known as a $O_2^{\bullet-}$-trapping agent and can effectively capture the $O_2^{\bullet-}$ generated in the reaction.[48] The material conduction band is more negative than the superoxide formation potential (Figure 2d); so, the material was expected to produce more superoxide radicals after illumination. The lowest amount of hydrogen peroxide is hence associated with the ability of the pBQ to quench superoxide radicals produced via the stepwise oxygen reduction reaction according to eq 9. This finding suggests that the oxygen reduction reaction for the formation of H_2O_2 could involve stepwise reactions involving radicals, as proposed below.

$$O_2 + e^- \rightarrow O_2^{\cdot-} \quad (9)$$

$$O_2^{\cdot-} + H^+ \rightarrow HO_2^{\cdot} \quad (10)$$

$$HO_2^{\cdot} + e^- \rightarrow HO_2^- \quad (11)$$

$$HO_2^- + H^+ \rightarrow H_2O_2 \quad (12)$$

These results can be associated with the fact that the synthesized CYANO−COF material oxidizes water to O_2 and reduces O_2 to produce H_2O_2 via a two-electron reaction as proposed in eqs 7 and 8; similar mechanism was also reported with some covalent organic materials.[49,50]

6. CONCLUSION

This study demonstrates the efficacy of an AB stacked model covalent organic framework synthesized from triformylphloroglucinol (Tp) and 4,4′-diamino-[1,1′-biphenyl]-3,3′-dicarbonitrile (Bp−CN) for photocatalytic hydrogen peroxide production via water splitting. This discovery aligns with green chemistry principles by eliminating the requirement for sacrificial electron donors, resulting in a more efficient and sustainable strategy for producing H_2O_2. The material demonstrated favorable photocatalytic performance under visible-light irradiation, highlighting the potential of COF-based materials in renewable energy applications. The material's architecture enabled effective charge separation and transfer, contributing to its high photocatalytic activity for H_2O_2 generation. While encouraging, this work emphasizes the need for more research into CYANO−COF catalysts' long-term stability and scalability. Future studies could focus on investigating cocatalysts or hybrid systems to increase efficiency. Overall, this study improves the science of photocatalysis while also opening up new paths for sustainable hydrogen peroxide synthesis, providing a greener alternative to traditional approaches.

■ ASSOCIATED CONTENT

Supporting Information

The Supporting Information is available free of charge at https://pubs.acs.org/doi/10.1021/acsomega.5c13395.

Experimental setup; strip test photographs; quantification of hydrogen peroxide production; solar-to-chemical conversion efficiency and apparent quantum yield calculations; powder XRD of simulated AB stacking mode and synthesized CYANO−COF; simulated stacking models; scanning electron microscopy images; photoelectrochemical characterization of the ligands; UV−vis spectra after different illumination times; hydrogen production rates over recycling cycles; hydrogen peroxide production tests using constituent ligands; effect of stirring; dark control experiments with scavengers; hydrogen peroxide production under direct sunlight; photocatalyst reusability study; and mechanistic investigations (PDF)

■ AUTHOR INFORMATION

Corresponding Authors

Ying Pan − *Department of Chemistry, Sustainable Materials Chemistry Group, University of Paderborn, 33098 Paderborn, Germany;* orcid.org/0000-0001-8156-397X; Email: ying.pan@uni-paderborn.de

Patrice Kenfack Tsobnang − *Department of Chemistry, Research Unit of Noxious Chemistry and Environmental Engineering, University of Dschang, Dschang 96, Cameroon;* orcid.org/0000-0002-1888-0099; Email: patrice.kenfack@univ-dschang.org

Nieves López-Salas − *Department of Chemistry, Sustainable Materials Chemistry Group, University of Paderborn, 33098 Paderborn, Germany;* orcid.org/0000-0002-8438-9548; Email: nieves.lopez.salas@uni-paderborn.de

Authors

Bernard Dawai − *Department of Chemistry, Research Unit of Noxious Chemistry and Environmental Engineering, University of Dschang, Dschang 96, Cameroon; Department of Chemistry, Sustainable Materials Chemistry Group, University of Paderborn, 33098 Paderborn, Germany;* orcid.org/0009-0005-0164-4494

Karlo Nolkemper − *Department of Chemistry, Theoretical Chemistry, and Center for Sustainable Systems Design, University of Paderborn, 33098 Paderborn, Germany;* orcid.org/0000-0002-5729-392X

Ignas Kenfack Tonle − *Department of Chemistry, Research Unit of Noxious Chemistry and Environmental Engineering, University of Dschang, Dschang 96, Cameroon;* orcid.org/0000-0001-9794-788X

https://doi.org/10.1021/acsomega.5c13395
ACS Omega 2026, 11, 22137−22147

Complete contact information is available at:
https://pubs.acs.org/10.1021/acsomega.5c13395

Author Contributions

B.D.: Investigation, methodology, formal analysis, and draft preparation; Y.P.: conceptualization, methodology, investigation, formal analysis, editing, supervision, and reviewing; K.N.: unit cell optimization and simulations. I.K.T.: supervision, reviewing, and editing; P.K.T.: methodology, formal analysis, supervision, reviewing, and editing. N.L.S.: conceptualization, resources, supervision, formal analysis, reviewing, editing, and writing—original draft.

Notes

The authors declare no competing financial interest.

■ ACKNOWLEDGMENTS

B.D. thanks the DAAD for financial support for the Short-term Research Grants, 2023 (57681230). N. López Salas also thanks DAAD for the AfriGER project (57703085) and UPB for internal funds support. Y.P. acknowledges financial support from the Postdoctoral Fellowship and Forschungs reserve Fund of the University of Paderborn. The authors acknowledge support for the publication cost by the Open Acess Publication Fund of Paderborn University.

■ REFERENCES

(1) Wang, Z.; Li, C.; Domen, K. Recent Developments in Heterogeneous Photocatalysts for Solar-Driven Overall Water Splitting. *Chem. Soc. Rev.* **2019**, *48* (7), 2109−2125.
(2) Liang, F.; Sun, X.; Hu, S.; Ma, H.; Wang, F.; Wu, G. Photocatalytic Water Splitting to Simultaneously Produce H_2 and H_2O_2 by Two-Electron Reduction Process Over Pt Loaded Na^+ Introduced g-C_3N_4 Catalyst. *Diam. Relat. Mater.* **2020**, *108*, 107971.
(3) Tan, D.; Zhuang, R.; Chen, R.; Ban, M.; Feng, W.; Xu, F.; Chen, X.; Wang, Q. Covalent Organic Frameworks Enable Sustainable Solar to Hydrogen Peroxide. *Adv. Funct. Mater.* **2024**, *34*, 1−24.
(4) Duca, G.; Travin, S. Reactions' Mechanisms and Applications of Hydrogen Peroxide. *Am. J. Phys. Chem.* **2020**, *9* (2), 36.
(5) Abdollahi, M.; Hosseini, A. Hydrogen Peroxide. *Encyclo. Tox.* **2014**, *2*, 967−970.
(6) Prasenjit, D.; Gouri, C.; Jérôme, R.; Sarah, V.; Jabor, R.; Arne, T. Integrating Bifunctionality and Chemical Stability in Covalent Organic Frameworks via One-Pot Multicomponent Reactions for Solar-Driven H_2O_2 Production. *J. Am. Chem. Soc.* **2023**, *145* (5), 2975−2984.
(7) Mase, K.; Yoneda, M.; Yamada, Y.; Fukuzumi, S. Seawater Useable for Production and Consumption of Hydrogen Peroxide as a Solar Fuel. *Nat. Commun.* **2016**, *7*, 1−7.
(8) Krishnaraj, C.; Sekhar Jena, H.; Bourda, L.; Laemont, A.; Pachfule, P.; Roeser, J.; Chandran, C. V.; Borgmans, S.; Rogge, S. M. J.; Leus, K.; Stevens, C. V.; Martens, J. A.; Van Speybroeck, V.; Breynaert, E.; Thomas, A.; Van Der Voort, P. Strongly Reducing (Diarylamino)benzene-Based Covalent Organic Framework for Metal-Free Visible Light Photocatalytic H_2O_2 Generation. *J. Am. Chem. Soc.* **2020**, *142* (47), 20107−20116.
(9) Shanley, E. S. Hydrogen Peroxide. *J. Chem. Educ.* **1951**, *28*, 260−266.
(10) Zhang, K.; Guo, L. Metal Sulphide Semiconductors for Photocatalytic Hydrogen Production. *Catal. Sci. Technol.* **2013**, *3* (7), 1672−1690.
(11) Rana, A.; Sudhaik, A.; Raizada, P.; Khan, A. A. P.; Van Le, Q.; Singh, A.; Selvasembian, R.; Nadda, A.; Singh, P. An Overview on Cellulose-Supported Semiconductor Photocatalysts for Water Purification. *Nanotechnol. Env. Eng.* **2021**, *6* (2), 40−38.
(12) Yong, Y.; Ma, T. Solar-to-H_2O_2 Catalyzed by Covalent Organic Frameworks. *Angew. Chemie-Int. Ed.* **2023**, *62* (49), 1−16.
(13) Sahoo, S. K.; Acharya, L.; Biswal, L.; Priyadarshini, P.; Parida, K. Recent Advancements in Graphitic Carbon Nitride Based Direct Z- and S-scheme Heterostructures for Photocatalytic H_2O_2 Production. *Inorg. Chem. Front.* **2024**, *11*, 4914.
(14) Li, Y.; Zhou, C.; Zhang, P.; Zhang, X.; Cao, Z.; Wang, Y.; Li, F.; Hu, C. Surface Electric Field-Induced Molecular Modification of Pollutants on Single-Atom Manganese Catalysts for Boosting Photocatalytic Water Purification and Simultaneous H_2O_2 Production. *J. Haz Mater.* **2025**, *494*, 138742−10.
(15) Zou, X.; Shi, Q.; Min, M.; Huang, D.; Zhang, G.; Wang, W.; Wang, G.; Liu, H.; Chen, Y.; Chen, A.; Deng, S. Metal−Organic Framework-Based Materials for Photocatalytic Hydrogen Peroxide Production: Insights into Mechanism, Modification Strategies, and Environmental Applications. *Adv. Energy Mater.* **2025**, 2501424.
(16) Akhtar, A.; Bidhan, K.; Avanti, C.; Bikash, M.; Samrat, G.; Arne, T.; Pradip, P. Covalent Organic Frameworks for Photocatalytic Hydrogen Peroxide Generation. *ACS Mater. Lett.* **2024**, *6* (5), 2007−2049.
(17) Pradip, P.; Amitava, A.; Jerome, R.; Thomas, L.; Michael, S.; Reinhard, S.; Arne, T.; Johannes, S. J. Diacetylene Functionalized Covalent Organic Framework (COF) for Photocatalytic Hydrogen Generation. *J. Am. Chem. Soc.* **2018**, *140* (4), 1423−1427.
(18) Zizhan, L.; Rongchen, S.; Yun, H. N.; Yang, F.; Tianyi, M.; Peng, Z.; Youji, L.; Xin, L. Covalent Organic Frameworks: Fundamentals, Mechanisms, Modification, and Applications in Photocatalysis. *Chem Catal.* **2022**, *2* (9), 2157−2228.
(19) Chien, I. Y.; Yee, S. T.; Hafiz, T. A. A.; Abdul, H.; Weng, P. W.; Rashmi, W.; Bey, H. G.; Mohammad, K. A Review on the Advancements in Covalent Organic Frameworks for Photocatalytic Reduction of Carbon Dioxide. *Coord. Chem. Rev.* **2024**, *521*, 216167.
(20) Islam, E. K.; Prasenjit, D.; Arne, T. Two-Dimensional Covalent Organic Frameworks: Structural Insights across Different Length Scales and Their Impact on Photocatalytic Efficiency. *Acc. Chem. Res.* **2024**, *57* (21), 3138−3150.
(21) Wang, K. H.; Hui, S. L.; Jia, X. F.; Xin, L.; Xiangmiao, Z.; Xiaodong, Y.; Jiangwei, Z.; Yuqin, J.; Hongliang, D.; Zhi, G. G. Targeted Construction of a Three-Dimensional Metal Covalent Organic Framework with Spin Topology for Photocatalytic Hydrogen Peroxide Production. *Chem. Eng. J.* **2022**, *449*, 137802.
(22) Zhao, H.; Yang, J.; Eisapour, M.; Hu, J.; Chen, Z. Photocatalytic Coproduction of Hydrogen Peroxide and Aldehydic/Keto Acid on Carbon Nitride. *Chem. Eng. J.* **2024**, *490*, 151767.
(23) Jiamin, S.; Himanshu, S. J.; Chidharth, K.; Kuber, S. R.; Sara, A.; Jeet, C.; Andreas, L.; Wanlu, L.; Hui, C.; Ying, Y. L.; Karen, L.; Henk, V.; Veronique, V. S.; Pascal, V. D. V. Pyrene-Based Covalent Organic Frameworks for Photocatalytic Hydrogen Peroxide. *Production..*
(24) Prasenjit, D.; Jérôme, R.; Arne, T. Solar Light Driven H_2O_2 Production and Selective Oxidations Using a Covalent Organic Framework Photocatalyst Prepared by a Multicomponent Reaction. *Angew. Chem., Int. Ed.* **2023**, *62*, 1−8.
(25) Croiset, E.; Rice, S. F.; Hanush, R. G. Hydrogen Peroxide Decomposition in Supercritical Water. *AIChE J.* **1997**, *43* (9), 2343−2352.
(26) Bamberger, C. E.; Brookhart, K.; Robinson, P. R. On the Thermal Decomposition of Trans-dibromotetraaquovanadium(III) bromide, $[VBr_2(H_2O)_4]Br{\cdot}2H_2O$. *Inorg. Chim. Acta* **1982**, *57* (C), 161−164.
(27) Samanta, C. Direct Synthesis of Hydrogen Peroxide from Hydrogen and Oxygen: An Overview of Recent Developments in the Process. *Appl. Catal. A Gen.* **2008**, *350* (2), 133−149.
(28) Hou, H.; Zeng, X.; Zhang, X. Production of Hydrogen Peroxide by Photocatalytic Processes. *Angew. Chemie-Int. Ed.* **2020**, *59* (40), 17356−17376.
(29) Xu, H.; Xia, S.; Li, C.; Li, Y.; Xing, W.; Jiang, Y.; Chen, X. Programming Tetrathiafulvalene-Based Covalent Organic Frame-

works for Promoted Photoinduced Molecular Oxygen Activation. *Angew. Chemie - Int. Ed.* **2024**, *63*, No. e202405476.
(30) Li, C.; Liu, J.; Li, H.; Wu, K.; Wang, J.; Yang, Q. Covalent Organic Frameworks with High Quantum Efficiency in Sacrificial Photocatalytic Hydrogen Evolution. *Nat. Commun.* **2022**, *13* (1), 1−9.
(31) Mengyun, W.; Shiyi, Q.; Haoyu, Y.; Yixin, H.; Lin, D.; Bilin, Z.; Jing, Z. Spectrophotometric Determination of Hydrogen Peroxide in Water with Peroxidase-Catalyzed Oxidation of Potassium Iodide and its Applications to Hydroxylamine-Involved Fenton and Fenton-Like Systems. *Chemosphere* **2021**, *270*, 129448.
(32) Kireev, S. V.; Shnyrev, S. L. Study of Molecular Iodine, Iodate Ions, Iodide Ions, and Triiodide Ions Solutions Absorption in the UV and Visible Light Spectral Bands. *Laser Phys.* **2015**, *25* (7), 075602.
(33) Xie, Q.; Chen, A.; Li, X.; Xu, C.; Bi, S.; Zhang, W.; Tang, J.; Pan, C.; Zhang, F.; Yu, G. Tuning the Interlayer Stacking of a Vinylene-Linked Covalent Organic Framework for Enhancing Sacrificial Agent-Free Hydrogen Peroxide Photoproduction. *Chem. Sci.* **2025**, *16*, 2215.
(34) Li, K. H.; Liu, L. N.; Xue, Z. X.; Xu, Z. W.; Gawale, Y.; Zhao, F.; Li, W. S. Interlayer-Stacking Mode Modulation in an Imine Covalent Organic Framework for Efficient Photocatalytic Hydrogen Production. *J. Mater. Chem. A* **2025**, *13*, 27661−27672.
(35) Deng, M.; Sun, J.; Laemont, A.; Liu, C.; Wang, L.; Bourda, L.; Chakraborty, J.; Van Hecke, K.; Morent, R.; De Geyter, N.; et al. Extending the π-Conjugation System of Covalent Organic Frameworks for more Efficient Photocatalytic H_2O_2 Production. *Green Chem.* **2023**, *25*, 3069−3076.
(36) Tayebi, M.; Masoumi, Z.; Lee, B. K. Ultrasonically Prepared Photocatalyst of W/WO_3 Nanoplates with WS_2 Nanosheets as 2D Material for Improving Photoelectrochemical Water Splitting. *Ultrason. Sonochem.* **2021**, *70*, 105339.
(37) Rosemary, J.; Giulio, D. 'A.; Payam, S.; Foqia, R.; Joachim, S. AP-XPS Study of Ethanol Adsorption on Rutile TiO_2(110). *J. Phys. Chem. C* **2022**, *126* (39), 16894−16902.
(38) Eva, P.; José, A. A.; Xavier, D.; José, P. TiO_2 deactivation during gas-phase photocatalytic oxidation of ethanol. *Catal. Today* **2002**, *76*, 259−270.
(39) Commentary, G. Undesired Role of Sacrificial Reagents in Photocatalysis. *J. Phys. Chem. Lett.* **2013**, *4*, 3479−3483.
(40) Vignesh, K.; Muhammad, D. I.; Ahmed, B.; Rama, K. C.; Jeong, Y. D.; Misook, K.; Ahmed, A. W. Photocatalytic Hydrogen Production: Role of Sacrificial Reagents on the Activity of Oxide, Carbon, and Sulfide Catalysts. *Catalysts* **2019**, *9*(3)..
(41) Yi, M.; Xiaodong, W.; Chencheng, Q.; Junying, C.; Yanlan, Z.; Longbo, J.; Chen, Z.; Xingzhong, Y.; Edison, H. A.; Hou, W. Linkage Microenvironment of Azoles-Related Covalent Organic Frameworks Precisely Regulates Photocatalytic Generation of Hydrogen Peroxide. *Angew. Chem., Int. Ed.* **2023**, *62*, 1−10.
(42) Yixue, X.; Fan, Q.; Yubin, F.; Shun-Feng, L.; Xing, S.; Kunquan, H.; Mei-Mei, Z.; Xin, Z.; Yuqiao, W.; Shun-Qi, X. Solvent-Driven Precise Control of Stacking Configurations in Covalent Organic Frameworks for High-Efficiency Photocatalysis. *Angew. Chem., Int. Ed.* **2025**, *64*, 1−10.
(43) Kang, C.; Zhang, Z.; Wee, V.; Usadi, A. K.; Calabro, D. C.; Baugh, L. S.; Wang, S.; Wang, Y.; Zhao, D. Interlayer shifting in two-dimensional covalent organic frameworks. *J. Am. Chem. Soc.* **2020**, *142* (30), 12995−13002.
(44) Zhang, Y.; Položij, M.; Heine, T. Statistical Representation of Stacking Disorder in Layered Covalent Organic Frameworks. *Chem. Mater.* **2022**, *34*, 2376−2381.
(45) Qingyao, W.; Jingjing, C.; Xiao, W.; Yan, L.; Yajie, Z.; Hui, W.; Yang, L.; Hui, H.; Fan, L.; Mingwang, S.; Zhenghui, K. A Metal-Free Photocatalyst for Highly Efficient Hydrogen Peroxide Photoproduction in Real Seawater. *Nat. Commun.* **2021**, *12*(1)..
(46) Trenczek-Zajac, A.; Synowiec, M.; Zakrzewska, K.; Zazakowny, K.; Kowalski, K.; Dziedzic, A.; Radecka, M. Scavenger-Supported Photocatalytic Evidence of an Extended Type I Electronic Structure of the TiO_2@Fe_2O_3 Interface. *ACS Appl. Mater. Interfaces* **2022**, *14* (33), 38255−38269.
(47) Zhou, E.; Wang, F.; Zhang, X.; Hui, Y.; Wang, Y. Cyanide-Based Covalent Organic Frameworks for Enhanced Overall Photocatalytic Hydrogen Peroxide Production. *Angew. Chemie-Int. Ed.* **2024**, *63* (19), 1−6.
(48) Zhang, N.; Lin, S.; Wang, F.; Liu, Y.; Zhang, J.; Zhou, L.; Lei, J. Highly Efficient Photocatalytic - H_2O_2 Production. *Res. Chem. Intermed.* **2021**, *47* (8), 3379−3393.
(49) Chen, D.; Chen, W.; Wu, Y.; Wang, L.; Wu, X.; Xu, H.; Chen, L. Covalent Organic Frameworks Containing Dual O_2 Reduction Centers for Overall Photosynthetic Hydrogen Peroxide Production. *Angew. Chemie-Int. Ed.* **2023**, *62* (9), 1−9.
(50) Zhai, L.; Xie, Z.; Cui, C. X.; Yang, X.; Xu, Q.; Ke, X.; Liu, M.; Qu, L. B.; Chen, X.; Mi, L. Constructing Synergistic Triazine and Acetylene Cores in Fully Conjugated Covalent Organic Frameworks for Cascade Photocatalytic H_2O_2 Production. *Chem. Mater.* **2022**, *34*, 5232−5240.
(51) Chen, L.; Wang, L.; Wan, Y.; Zhang, Y.; Qi, Z.; Wu, X.; Xu, H. Acetylene and Diacetylene Functionalized Covalent Triazine Frameworks as Metal-Free Photocatalysts for Hydrogen Peroxide Production: A New Two-Electron Water Oxidation Pathway. *Adv. Mater.* **2020**, *32* (2), 1−10.
(52) Zhao, W.; Yan, P.; Li, B.; Bahri, M.; Liu, L.; Zhou, X.; Clowes, R.; Browning, N. D.; Wu, Y.; Ward, J. W.; Cooper, A. I. Accelerated Synthesis and Discovery of Covalent Organic Framework Photocatalysts for Hydrogen Peroxide Production. *J. Am. Chem. Soc.* **2022**, *144* (22), 9902−9909.
(53) Chang, X.; Yang, J.; Han, D.; Zhang, B.; Xiang, X.; He, J. Enhancing Light-Driven Production of Hydrogen Peroxide by Anchoring Au onto C_3N_4 Catalysts. *Catalysts* **2018**, *8* (4), 147−13.
(54) Burek, B. O.; Bahnemann, D. W.; Bloh, J. Z. Modeling and Optimization of the Photocatalytic Reduction of Molecular Oxygen to Hydrogen Peroxide over Titanium Dioxide. *ACS Catal.* **2019**, *9* (1), 25−37.
(55) Shiraishi, Y.; Takii, T.; Hagi, T.; Mori, S.; Kofuji, Y.; Kitagawa, Y.; Tanaka, S.; Ichikawa, S.; Hirai, T. Resorcinol−Formaldehyde Resins as Metal-Free Semiconductor Photocatalysts for Solar-to-Hydrogen Peroxide Energy Conversion. *Nat. Mater.* **2019**, *18* (9), 985−993.
(56) Thakur, S.; Kshetri, T.; Kim, N. H.; Lee, J. H. Sunlight-Driven Sustainable Production of Hydrogen Peroxide using a CdS−Graphene Hybrid Photocatalyst. *J. Catal.* **2017**, *345*, 78−86.

https://doi.org/10.1021/acsomega.5c13395
ACS Omega 2026, 11, 22137−22147